Nanoscale

PAPER

View Article Online
View Journal | View Issue

Cite this: *Nanoscale*, 2021, **13**, 19568

pH-Dependent interaction mechanism of lignin nanofilms†

Seo Yoon Lee, [a] Jinhoon Lee, [a] Yoojung Song,[a,b] Markus Valtiner[c] and Dong Woog Lee *[a]

Lignin has been spotlighted as an abundant renewable bioresource for use in material technologies and applications such as biofuels, binders, composites, and nanomaterials for drug delivery. However, owing to its complex and irregular structure, it is difficult to investigate its fundamental interaction mechanism, which is necessary to promote its use. In this study, a surface forces apparatus (SFA) was used to investigate the pH-dependent molecular interactions between a lignin nanofilm and five functionalized self-assembled monolayers (SAMs). The lignin nanofilm adhered most strongly to the amine-functionalized SAM, indicating that the molecular interactions with lignin were mainly electrostatic and cation–π interactions. The force–distance profile between lignin and a methyl-functionalized SAM revealed pH-dependent interactions similar to those between two lignin nanofilms. This finding indicates that the dominant cohesion mechanism is hydrophobic interactions. A quartz crystal microbalance with dissipation was used to investigate the adsorption of free lignin molecules on functionalized SAMs. Lignin molecules, which were free in solution, were most effectively adsorbed to the phenyl-functionalized SAM. To investigate whether the nanoscopic interaction forces could be extended to macroscopic properties, the compressive strength of activated carbon–lignin composites prepared at different pH values was evaluated. As the pH increased, the compressive strength decreased owing to the reduced hydrophobic interactions between the activated carbon and lignin, consistent with the SFA results. These quantitative results regarding lignin interactions can advance the potential use of lignin as an eco-friendly biomaterial.

Received 15th September 2021,
Accepted 15th November 2021

DOI: 10.1039/d1nr06076g

rsc.li/nanoscale

Introduction

Concerns regarding the environmental deterioration caused by advancements in industrial technologies have promoted the development of eco-friendly biomaterials that can replace fossil-fuel-based synthetic polymers. Therefore, natural biopolymers from plant biomass have emerged as alternatives owing to their biodegradable, environmentally friendly, cost-effective, and renewable characteristics. Lignin, the second most abundant biopolymer in nature, accounts for 15–30% of the composition of wood, and is necessary for the formation of plant cell walls with cellulose and hemicellulose.[1] Although lignin is a byproduct of the pulp and paper industries,[2] it exhibits versatile characteristics such as aromaticity,[3] multi-functionality,[4] biocompatibility,[5] and reinforcing capability.[6] Thus, the use of lignin has been considered for various applications such as dispersants, adhesives, biofuels, drug delivery, and nanocomposites.[7–13] However, owing to the complex bonds and macromolecular structures of lignin, which depend on the botanical origin and extraction procedure, only ~2% of the 50 million tons of lignin generated in 2014 has been utilized for value-added applications.[10,14,15]

Several researchers have attempted to convert lignin into valuable materials by using techniques such as depolymerization[16] and chemical modification,[17] and by synthesizing it into colloidal particles.[18] However, the transformation of lignin into high-value products remains challenging owing to the lack of fundamental information on the lignin binding mechanism. Clarifying various interactions with lignin is thus important for commercializing lignin-derived products.

In this study, the interaction mechanism of lignin nanofilms was extensively investigated using a surface forces apparatus (SFA), which was adopted to determine the interaction forces and molecular mechanism between two surfaces with distance and force resolutions of 0.1 nm and 10 nN, respectively.[19] We used alkaline lignin extracted mainly from the wood of needle-leaved pine trees. The lignin that we used was previously subjected to a sulfonate (SO_3^-) treatment to make it

[a]*School of Energy and Chemical Engineering, Ulsan National Institute of Science and Technology (UNIST), Ulsan, 44919, Republic of Korea.*
E-mail: dongwoog.lee@unist.ac.kr
[b]*Make-up Lab., Kolmar Korea, Seoul, 06792, Republic of Korea*
[c]*Vienna University of Technology, Institute of Applied Physics, Wiedner Hauptstrasse 8-10, A-1040, Vienna, Austria*

†Electronic supplementary information (ESI) available. See DOI: 10.1039/d1nr06076g

soluble in water.[20,21] Interaction forces were measured between lignin nanofilms and five functionalized self-assembled monolayers (SAMs), namely, hydroxyl (OH-), carboxylic (COOH-), phenyl (C_6H_5-), methyl (CH_3-), and amine (NH_2-)-functionalized SAMs, at various pH conditions (pH 2, 4, 7, and 10). Subsequently, the pH-dependent cohesion force between two lignin nanofilms was directly measured to clarify the inherent interaction mechanism among lignin molecules through a comparison with the interaction forces between lignin and functionalized SAMs. In addition to the SFA measurement, an analysis was performed using a quartz crystal microbalance with dissipation (QCM-D) to evaluate the adsorption of free lignin molecules (dissolved in a solution) on surfaces with different functional groups. Furthermore, to examine the significance of nanoscopic and interfacial adhesion forces for determining the macroscopic and bulk properties, lignin-reinforced activated carbon composites were synthesized and evaluated. The comprehensive and quantitative analysis on a nano-to-bulk scale can help enhance the understanding of the fundamental mechanism underlying molecular interactions in lignin to promote its applications.

Experimental section

Preparation of functionalized SAM surfaces

To prepare a molecularly smooth gold surface, which has a low root-mean-square roughness of <0.2 nm, gold (~45 nm) was deposited onto freshly cleaved muscovite mica (grade #1, S&J Trading, Floral Park, NY, USA) with a uniform surface *via* electron beam evaporation.[22] The gold-coated mica was adhered to cylindrical disks (radius of curvature, R = 2 cm), gold side down, using an optical adhesive (NOA 81, Norland Products, NJ, USA), followed by UV curing for ~50 min using a UV lamp (UVP B-100AP, AnalytikJena, Germany). The mica was then carefully detached to obtain the molecularly smooth and clean gold layer.[23]

To deposit OH-, COOH-, C_6H_5-, CH_3-, and NH_2-functionalized SAMs onto the prepared gold surfaces, the following alkanethiol solutions (1 mM in ethanol) were prepared: 11-hydroxy-1-undecanethiol (97%), 10-carboxy-1-decanethiol (95%), 2-phenylethanethiol (98%), 1-undecanethiol (98%), and 11-amino-1-undecanethiol hydrochloride (99%), respectively, purchased from Sigma-Aldrich (St Louis, MO, USA). Specifically, the prepared gold surfaces were separately immersed in each target alkanethiol solution for ~18 h. Finally, each SAM-coated disk was weakly sonicated to remove unbound and/or loosely bound molecules, followed by drying with N_2 blowing.

Preparation of lignin films

Sulfonate-treated alkaline lignin (Bonding Chemical, Katy, TX, USA) was dissolved in deionized (DI) water (10 μg mL^{-1}) and filtered using a 0.2 μm polytetrafluoroethylene (PTFE) filter (ADVANTEC) to remove aggregates and impurities. Freshly cleaved and back-silvered mica[19] was attached on a cylindrical disk using the same NOA 81 optical adhesive with UV curing for ~60 min using the same UV UVP B-100AP lamp. The prepared lignin solution was drop-casted onto the mica surface and remained for ~40 min, followed by washing with DI water to remove the unbound molecules.

Preparation of pH buffer solution

For the SFA measurement, four buffer solutions with different pH values (2, 4, 7, and 10) were used to clarify the pH dependence of lignin interaction force. The Buffer Maker program (Version 1.1.0.0; BPP Marcin Borkowski©, 2008) was used to set the individual amounts of HNO_3, NaOH, and $NaNO_3$. To eliminate the effect of salt concentration on the interaction force, the total ion strength was set as 50 mM (ESI Table S1†).

Zeta potential measurement

Lignin was dissolved in water (0.5 wt%), and HNO_3 or NaOH was injected to control the pH to the target value. Zeta potentials were measured using a Malvern Zetasizer Nano ZS (Malvern, Worcestershire, UK). Each measurement was repeated at least three times.

Interaction force measurements using SFA

The interaction forces between pairs of surfaces, both asymmetric (lignin *vs.* SAM) and symmetric (lignin *vs.* lignin) pairs, were measured using an SFA (SFA 2000, Surforce LLC, USA).[19] Each cylindrical disk was placed in the SFA chamber with crossed geometry. Then the prepared buffer solutions with different pH values (2, 4, 7, and 10) were injected between the two opposing surfaces. After 30 min of equilibration, the surfaces were moved toward each other at a constant rate (~5 nm s^{-1}) until reaching full contact. After a brief contact time (~5 s), the surfaces were retracted and the interaction forces were measured by the deflection of double cantilevered spring (spring constant, k = 2451.7 N m^{-1}) connected to the lower cylindrical disk. The absolute distance (D) and force (F) were computed

Dong Woog Lee

Professor Dong Woog Lee received his BS in Chemical and Biomolecular Engineering at Korea Advanced Institute of Science and Technology (KAIST) in 2008 and his PhD in Chemical Engineering from the University of California, Santa Barbara (UCSB) in 2014 under the supervision of Professor Jacob Israelachvili. He continued his work in the same lab for two more years as a postdoctoral researcher (2014–2016), and is currently an Associate Professor at Ulsan National Institute of Science and Technology (UNIST). His research focuses on studying fundamental interaction forces between bio/biomimetic molecules (biomolecules, polymers, proteins, lipid membranes) using a Surface Forces Apparatus (SFA), and applying them to valuable materials (polymer composites, adhesives, coatings, lubricants).

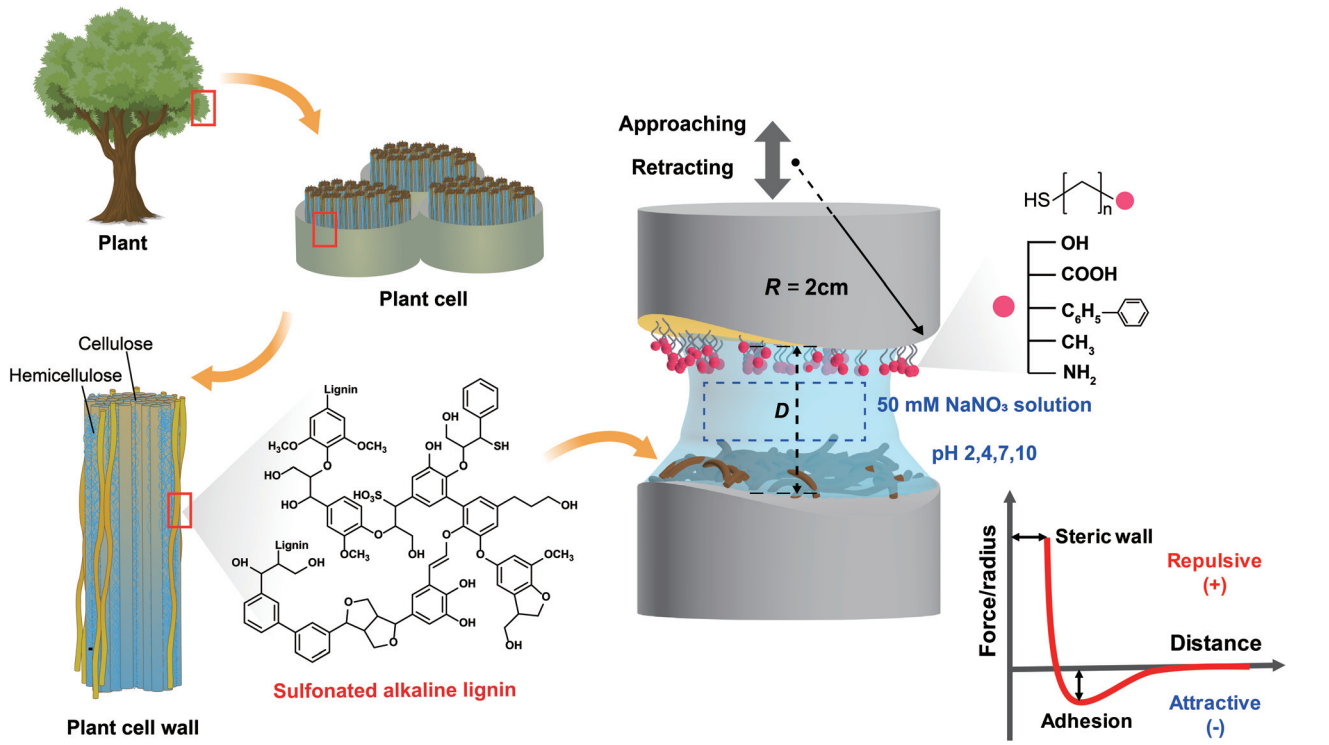

Fig. 1 Schematic of surface forces apparatus (SFA) for measuring the interaction forces between two surfaces: self-assembled monolayers (SAMs) separately functionalized by five different alkanethiols (top surface) and sulfonated alkaline lignin from lignocellulosic biomass (bottom surface). Between the surfaces, a 50 mM $NaNO_3$ solution was injected, and the force was measured at pH 2, 4, 7, and 10. From the measured interaction force profile between the SAMs and lignin, the adhesion force (energy) and steric wall thickness could be obtained.

using multiple beam interferometry (MBI) through fringes of equal chromatic order (FECO).[19] The adhesion energy (W_{ad}) was evaluated by applying the Johnson–Kendall–Roberts (JKR) model, defined as $W_{ad} = 2F_{ad}/3\pi R$, where F_{ad} is the absolute value of lowest interaction force (F) before jump-out (when the surfaces are not purely repulsive).[19,24] All experiments were conducted at least three times at the same point, and the results of three samples were considered to ensure the reliability of the data. A schematic of the SFA measurement is described in Fig. 1.

QCM-D analysis

QCM-D analysis was performed using a Q-Sense E4 operator (Biolin Scientific Q-Sense, Stockholm, Sweden) and gold-coated sensors (QSensor QSX30 Gold, Biolin Scientific). Before the measurement, the sensors were cleaned to remove any contamination and dust according to the following procedure: (i) UV/ozone treatment for 10 min, (ii) immersion of the sensors in a heated 5 : 1 : 1 mixture of H_2O/NH_3 (25%)/H_2O_2 (30%) for 5 min at 75 °C, (iii) rinsing with DI water followed by drying with N_2, and (iv) UV/ozone treatment for 10 min. After cleaning, the sensors were separately immersed in each alkanethiol solution (1 mM in ethanol) for ~18 h, followed by weak sonication and rigorous washing with ethanol to remove unbound and weakly bound molecules.

The QCM-D analysis was conducted in the following order at a flowrate of 0.5 mL min^{-1}: (i) a pH 7 buffer solution to obtain the baseline, (ii) a 1 mg mL^{-1} lignin solution to obtain the amounts of lignin initially adsorbed on the surface, and (iii) a pH 7 buffer solution to wash off the unbound or weakly bound lignin over the SAM-coated surface.

The amounts of initially adsorbed lignin and lignin remaining after washing were evaluated (Fig. 4a) using the Sauerbrey equation:

$$\Delta F = -C_f \times \Delta m,$$

where ΔF is the change in the resonance frequency (Hz), C_f is the sensitivity factor of the crystal, and Δm is the changes in the mass per unit area (μg cm^{-2}).[25] The seventh overtone was selected to represent the overall QCM-D results, and the average adsorbed mass was obtained by converting the frequencies of the third, fifth, and seventh overtones into mass values. All QCM-D measurements were performed at 25 °C.

Activated carbon–lignin composites

Activated carbon (activated charcoal powder, CAS no. 7440-44-0, pH 5.0–8.0, specific gravity 0.08–0.5, water solubility <0.5%, SAMCHUN, Republic of Korea) and alkaline lignin, at a ratio of 90 : 10 wt%,[20] were dissolved in 50 mM buffer solutions with pH values of 2, 4, 7, and 10, followed by vortexing for ~30 s. Each prepared slurry was poured into a custom-made steel cylindrical mold (diameter and height of 12 mm and 24 mm, respectively). The slurry was dried at 25 °C for 24 h and then 80 °C in dry oven for 24 h to obtain a columnar activated carbon–lignin composite (ESI Fig. S1†).

Compressive strength measurement of activated carbon–lignin composite

To investigate the strength of activated carbon–lignin composites, a universal testing machine (WL2100, WITHLAB. Co., Republic of Korea) was used to measure the compressive strength, as defined by ASTM D 695. A cylindrical compressive jig (diameter and height of 100 mm and 20 mm, respectively) was used to perform the examinations at a constant compression rate of 1.3 mm min^{-1}. The compressive strength was typically measured at the load before failure.

Results and discussion

For a typical force–distance profile measured by the SFA experiments, pieces of important information can be obtained: (i) the interaction force at a specific mica–mica distance where positive and negative interaction forces indicate repulsion and adhesion between the two surfaces, respectively; (ii) electrostatic and/or steric repulsion between two layers, which can be demonstrated through the in-curve (*i.e.*, approaching curve) profiles; (iii) the minimum force in the out-curve (retracting curve), which indicates the adhesive or cohesive force between two surfaces and is recorded by the deflection of a double cantilever spring attached on the lower surface; (iv) steric (hard) wall, which represents the thickness of layers, as measured by the mica–mica distance (in this work, the sum of thicknesses of SAM layer and lignin nanofilm). In this work, the specific chemistry of SAMs can readily be determined at each pH through their known pK_a values (ESI Table S2†). Thus, we can expect a specific interaction depending on the types of SAMs at each pH condition, as explained in the Results and discussion section for each SAM.

The interaction forces between the lignin nanofilm and each functionalized SAM surface were measured using the SFA to determine and quantify the dominant interaction (see the Experimental section for the sample preparation protocol). The force–distance profiles during the approach and retraction of the lignin and SAM surfaces were measured to determine adhesion force (energy) under various conditions. These measurements were conducted in a 50 mM $NaNO_3$ buffer solution at pH 2, 4, 7, and 10. Notably, the pH adjusts the charge of both lignin and the SAMs; thus, a wide range of pH values was employed to investigate the pH-dependence of the force–distance profiles owing to electrostatic interactions and various π-interactions (*i.e.*, cation–π, π–π). Fig. 2a–e show the force–distance profiles between lignin and five functionalized SAMs under different pH conditions, and the resulting adhesion energies are summarized in Fig. 2f.

Interaction force between lignin nanofilm and OH-SAM

OH-SAM (11-hydroxy-1-undecanethiol) has a pK_a value of 16–18 so it could function as hydrogen bonding donor and acceptor under a wide range of pH conditions (below ~pH 16) (ESI Table S2†). Consequently, any changes in the interaction profile could be considered as due to transition of lignin. The force–distance curves indicate that the interactions between lignin and OH-SAM were mostly governed by steric repulsion at all pH conditions. In general, as the pH increases, lignin becomes more negatively charged (ESI Fig. S2†) and hydrophilic owing to the deprotonation of the lignin functional groups such as sulfonate (pK_a ~ 2), carboxylic (pK_a ~ 5), and hydroxyl groups (pK_a ~ 10).[26,27] Thus, at high pH values, the lignin became less adhesive to the negatively charged mica,[28] thereby forming a more swollen structure (ESI Fig. S3†) which caused the higher steric repulsion and steric wall (D_{sw}, defined as the D at F/R ~ 40 mN m^{-1}) compared to those at a low pH values. Although lignin has several hydrogen bond donating (*i.e.*, hydroxyl and carboxyl) and accepting groups (*i.e.*, hydroxyl, carboxyl, and carbonyl), the negligible adhesion with OH-SAM demonstrates that the contribution of the hydrogen bonding to lignin binding is not as significant as previous work.[29]

Interaction force between lignin nanofilm and COOH-SAM

COOH-SAM (10-carboxy-1-decanethiol) has a pK_a value of ~5.5 (ESI Table S2†). Thus, the –COOH is maintained at a low pH (<5.5), whereas $–COO^-$ forms at a high pH (>5.5) owing to deprotonation. Thus, carboxylic groups can function as hydrogen bond donors and acceptors at a low pH, but only as hydrogen bond acceptors at a high pH. Moreover, at a high pH value, the anionic charge of $–COO^-$ can induce the electrostatic interactions with the negatively charged lignin. According to the force–distance profiles (Fig. 2b), a weak adhesion was observed at pH 2 owing to the hydrogen bond formation between COOH-SAM and the hydrophilic functional groups on lignin (*i.e.*, carboxylic, carbonyl and hydroxyl). From the profile, the adhesion between OH-SAM and lignin could not be measured, although a certain adhesion could be achieved owing to the larger number of hydrogen bonding sites on COOH-SAM than those on OH-SAM (W_{ad} = 0.32 ± 0.13 mJ m^{-2} at pH 2.0). At a higher pH, the steric repulsion from the swelled lignin (D_{sw} ~ 5.0 nm at pH 10) and electrostatic repulsion between the deprotonated $–COO^-$ and negatively charged lignin overcame the adhesive hydrogen bonding, representing a purely repulsive force profile. The results reinforce that the hydrogen bonding does not significantly affect the lignin adhesion, as in the case of OH-SAM.

Interaction force between lignin nanofilm and C_6H_5-SAM

Lignin consists of a large number of aromatic groups that can possibly interact *via* π–π interactions which has relatively low binding energy (~1.5–3 kcal mol^{-1}). Moreover, at a low pH, lignin exhibits a slight positive charge (ESI Fig. S2†) and can thus act as a cation source for cation–π interactions which has much larger binding energy (~9–23 kcal mol^{-1}).[30,31] To evaluate these possible interactions, C_6H_5-SAM (2-phenylethanethiol) was examined. Notably, its intrinsic hydrophobic property enables a certain amount of hydrophobic interactions. The force–distance curves show weak adhesion (W_{ad} = 0.14 ± 0.04 mJ m^{-2} at pH 2.0) which could be attributed to the

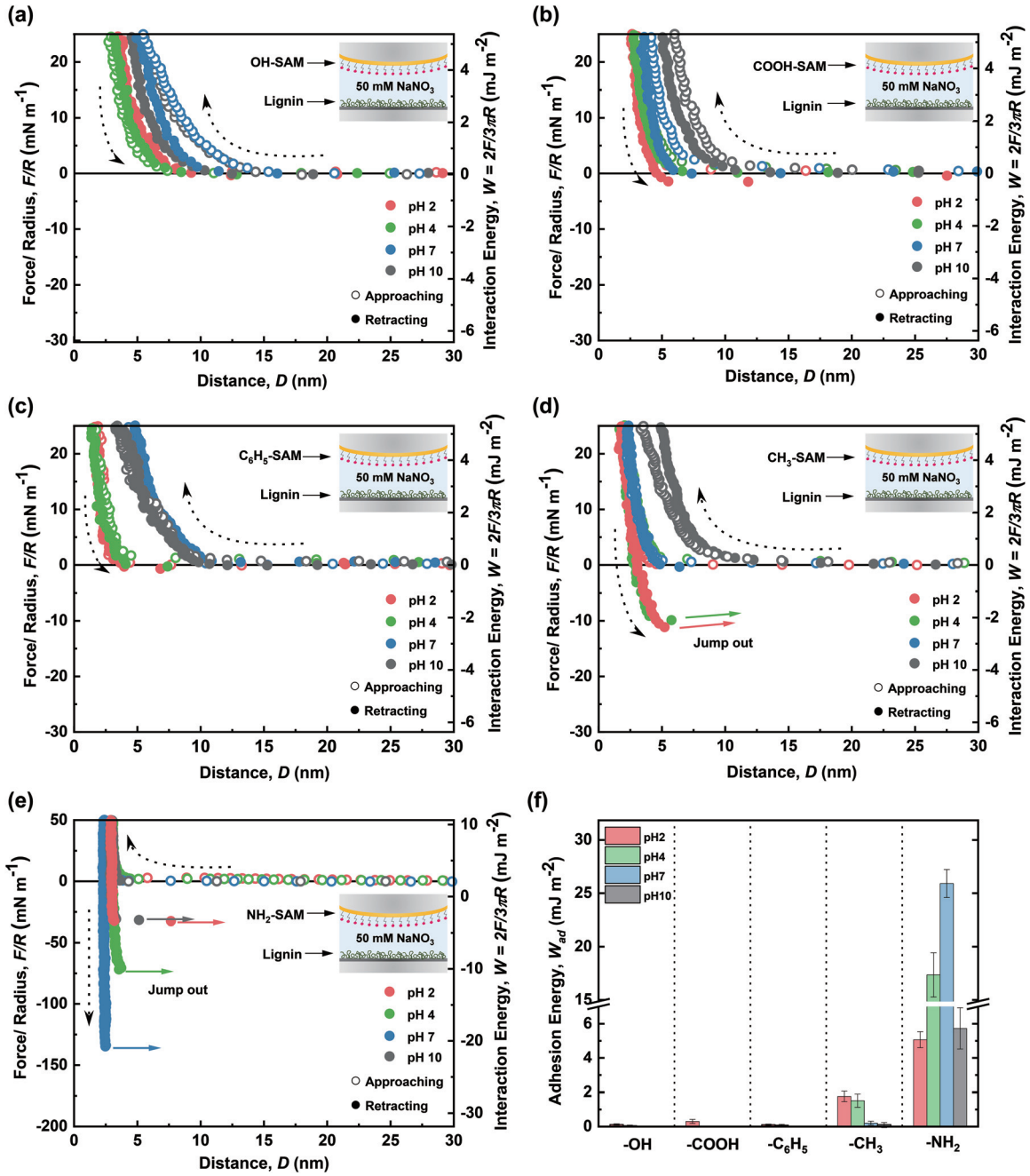

Fig. 2 Force–distance profiles between lignin nanofilms and SAMs terminated by various functional groups [(a) –OH, (b) –COOH, (c) $-C_6H_5$, (d) $-CH_3$, and (e) $-NH_2$] in pH 2, 4, 7, and 10 solutions. (f) Bar graph summarizing the overall adhesion energy (W_{ad}) for each curve.

cation–π interactions between the lignin and C_6H_5-SAM (Fig. 2c). However, no adhesion was measured under other pH conditions (in which the lignin was negatively charged). This finding indicates that π–π stacking is not an effective adhesion mechanism between lignin and C_6H_5-SAM. Owing to the swelling of the lignin structure, the steric wall ($D_{sw} \sim 3.0$ nm at pH 10) was noted to be increased toward the solution at high pH. Overall, the interactions of the lignin film *via* cation–π (when lignin act as the cation source) and π–π mechanisms were noted to be hindered at all pH values.

Interaction force between lignin nanofilm and CH_3-SAM

The interaction force measurement of lignin nanofilms with CH_3-SAM (1-undecanethiol) can help clarify hydrophobic interactions since the CH_3-SAM is known to be hydrophobic with a high water contact angle (~108°).[32] In the acidic condition, the adhesion energy (W_{ad} = 1.81 ± 0.32 mJ m^{-2} at pH 2.0) was significantly higher than those of OH-, COOH-, and C_6H_5-SAM, owing to the hydrophobic interactions between CH_3-SAM and lignin. As the pH increased to 10, the adhesion force almost

disappeared, and a purely repulsive force profile was observed. This phenomenon could be attributed to the decrease in the hydrophobicity of the lignin-coated surface as its charge increased (Fig. 2d). The results indicate that hydrophobic interactions dominate at pH 2 and 4, at which lignin conserves its hydrophobicity.

Interaction force between lignin nanofilm and NH_2-SAM

The amine group in NH_2-SAM (11-amino-1-undecanethiol hydrochloride) has a pK_a value of ~7.5 (ESI Table S2†). Therefore, the dominant forms are protonated amine ($-NH_3^+$) and $-NH_2$ at below and above pH 7.5, respectively. In acidic conditions, lignin can interact with NH_2-SAM *via* cation–π interactions as a π source, hydrogen bonding (as a hydrogen bond acceptor), and charge–charge interactions. Under basic conditions, deprotonation from $-NH_3^+$ to $-NH_2$ allows NH_2-SAM to function as both, hydrogen bonding donor and acceptor. As shown in Fig. 2e, the measured adhesion force between lignin and NH_2-SAM was the highest among those of functionalized SAMs (W_{ad} = 5.38 ± 0.56 mJ m^{-2} at pH 2.0). In addition, the adhesion energy increased with increasing pH, exhibiting the highest value among the functionalized SAMs at pH 7 (W_{ad} = 25.91 ± 3.09 mJ m^{-2}) and then, further increase with high pH (W_{ad} = 5.78 ± 1.02 mJ m^{-2} at pH 10.0). At pH 2, the cation–π interactions between the fully protonated amines and lignin aromatic rings induced strong adhesion, although it was slightly hindered by the extremely weak electrostatic repulsion between the positively charged amines and lignin. As the pH increased to 4, the still protonated amines and negatively charged lignin, resulting in cation–π interactions and electrostatic attraction, which enhanced the adhesion energy with respect to that at pH 2. Similarly, at pH 7, ~76% of the amines were protonated, and the lignin exhibited a stronger negative charge than pH 4 condition (ESI Fig. S2†). The maximization of the adhesion energy at pH 7 could be attributed to the balance between the positively charged amine and negatively charged lignin, which overcompensated for the slightly weaker cation–π interactions compared to those at a lower pH. Finally, as the pH increased to 10, most of the amines were in a neutral form, and the electrostatic attraction and cation–π interactions diminished, resulting in weaker adhesion. However, the residual positive charge ($-NH_3^+$) at pH 10 affected the higher adhesion energy between NH_2-SAM and lignin compared with that in the case of other SAMs. This finding indicates that the cation–π and even minimal electrostatic interactions significantly affect the lignin adhesion. Overall, the lignin nanofilm exhibited the highest adhesion energy against NH_2-SAM, which was dominated by cation–π interactions (when lignin act as a π source) and electrostatic interactions.

Interaction force between lignin nanofilms

In addition to the adhesion measurement, the cohesive interactions between lignin nanofilms (lignin *vs.* lignin) were investigated. Fig. 3a shows the force–distance curves between lignin-coated surfaces in different pH environments.

All the approach curves (in-curves) exhibited purely repulsive behaviors. To perform a more extensive analysis, the in-curves were fitted using an exponential decay formula (ESI Fig. S4†). The fitted decay lengths (λ^{-1} ~ 1.942 nm, ~1.916, and ~1.900 nm at pH 2, 4, and 7, respectively) were similar to the theoretical Debye length (κ^{-1} ~ 1.923 nm at 50 mM monovalent ion concentration)[33] except for that at pH 10 (λ^{-1} ~ 10.610 nm) (ESI Table S3†). In other words, electrostatic interactions primarily governed the long-range repulsion between lignin nanofilms during their approach in acidic and neutral pH conditions. In contrast, in the basic condition (pH 10), steric interactions owing to the swelling of lignin emerged as the dominant mechanism.

The highest cohesive energy between the lignin nanofilms was measured in acidic conditions (W_{ad} = 1.96 ± 0.32 and 1.61 ± 0.38 mJ m^{-2} at pH 2.0 and 4.0, respectively), and this energy decreased as the pH increased (W_{ad} ~ 0 mJ m^{-2} at both pH 7.0 and 10.0). The decrease in the cohesive energy with the

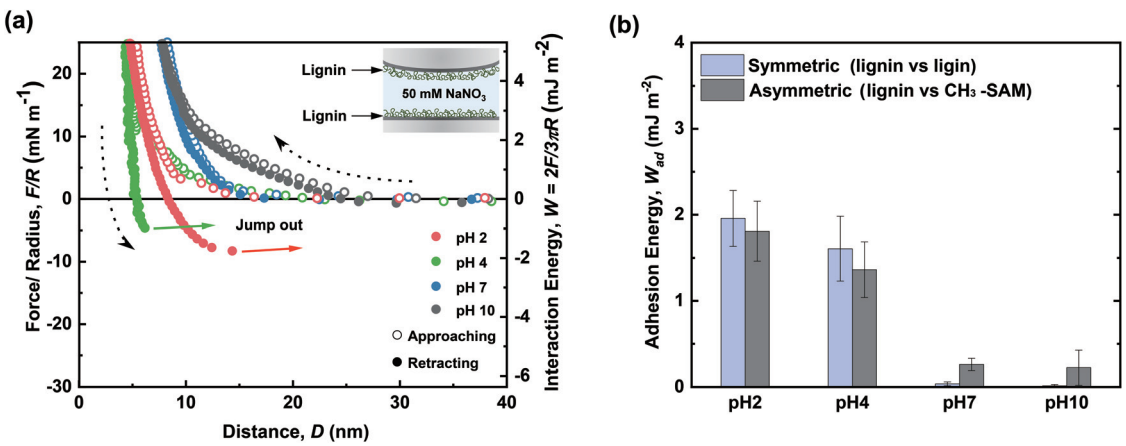

Fig. 3 Force–distance profiles for cohesion between lignin nanofilms in pH 2, 4, 7, and 10 solutions. (b) Comparison of cohesion energy (lignin *vs.* lignin) and adhesion energy (lignin *vs.* CH_3-SAM).

increase in pH could be attributed to (i) the increased electrostatic repulsion between lignin nanofilms, (ii) the swelling of the lignin nanofilms, which induced stronger steric repulsion, and (iii) the decreased hydrophobicity of the lignin nanofilms. The increase in the water solubility with increasing pH accounted for the decreased hydrophobicity, owing to which no aggregation or precipitation occurred at pH 7 or pH 10 (ESI Fig. S5†). Moreover, the magnitudes of the cohesive strength and decreasing cohesion tendency with increasing pH were similar to those in the asymmetric case (CH_3-SAM *vs.* lignin) (Fig. 3b). Therefore, the interactions governing cohesion between lignin layers were expected to be hydrophobic, which is consistent with previously reported results.[20]

QCM-D measurement

To investigate the adsorption of lignin molecules on the SAM-coated surfaces in the free-in-solution state, QCM-D measurements were performed. Fig. 4 shows the adsorbed lignin at each surface, represented by mass and converted from frequency shifts (ESI Fig. S6†).

The C_6H_5-SAM surface initially adsorbed the highest mass of lignin (~174.1 ng cm^{-2}), and the greatest amount remained after washing (~118.6 ng cm^{-2}) (Fig. 4b). This result was in contrast with the SFA result, which exhibited a relatively low adhesion energy between lignin and C_6H_5-SAM. Free lignin in the solution (with a high mobility and rotational freedom) and lignin which adhered to the surface appeared different adhesion mechanisms. In general, for the case of π–π interactions between C_6H_5-SAM and lignin, the arrangement of benzene rings in lignin is significant. However, in case of fixed lignin, *i.e.*, when it was fixed onto mica, the π–π interactions did not effectively occur, possibly owing to the low mobility of lignin. Alternatively, when the lignin is adsorbed onto mica surface, a structure could be formed that hinders π–π interactions with external molecules. Furthermore, the adhesion energy owing to hydrogen bonds was barely detected in the SFA measurements (W_{ad} ~ 0 mJ m^{-2} for OH-SAM and COOH-SAM at pH 7.0) was observable in the QCM-D measurements (~7.6 and 28.3 ng cm^{-2} for OH-SAM and COOH-SAM at pH 7.0). This finding indicates that hydrogen bond donors and acceptors are considerably more accessible in a system with free lignin. As in the SFA results, the lignin molecules could be effectively adsorbed onto the NH_2-SAM surface (~155.6 ng cm^{-2}), and a significant amount remained even after washing with a buffer (~95.3 ng cm^{-2}). Initially, the lignin appeared to effectively adsorb on CH_3-SAM (~125.7 ng cm^{-2}) *via* hydrophobic interactions, but after washing, only a limited amount of lignin remained on the surface (~43.7 ng cm^{-2}), which is consistent with the SFA analysis at pH 7.

Lignin interaction mechanism

The SFA and QCM-D results clarified possible interaction mechanisms of lignin nanofilms (coated on the surface) and lignin molecules (in the solution) (Fig. 5). According to the

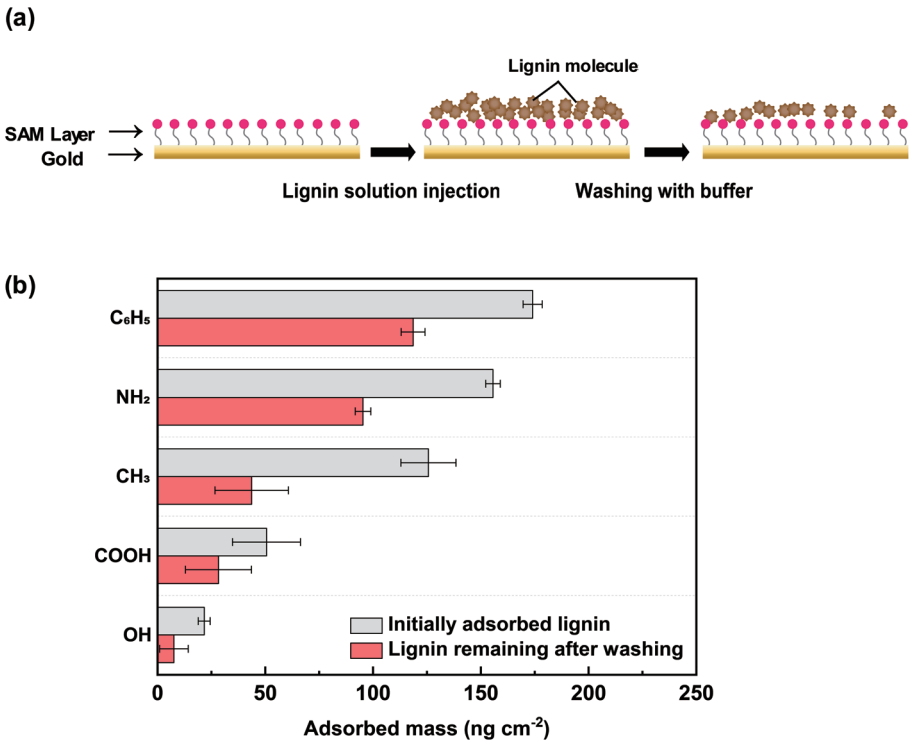

Fig. 4 Lignin molecules adsorbed on SAM-coated gold surface monitored *via* QCM-D analysis. (a) Schematic of lignin molecules at the gold sensor surface. (b) Calculated adsorbed and remaining mass of lignin molecules on each functionalized surface.

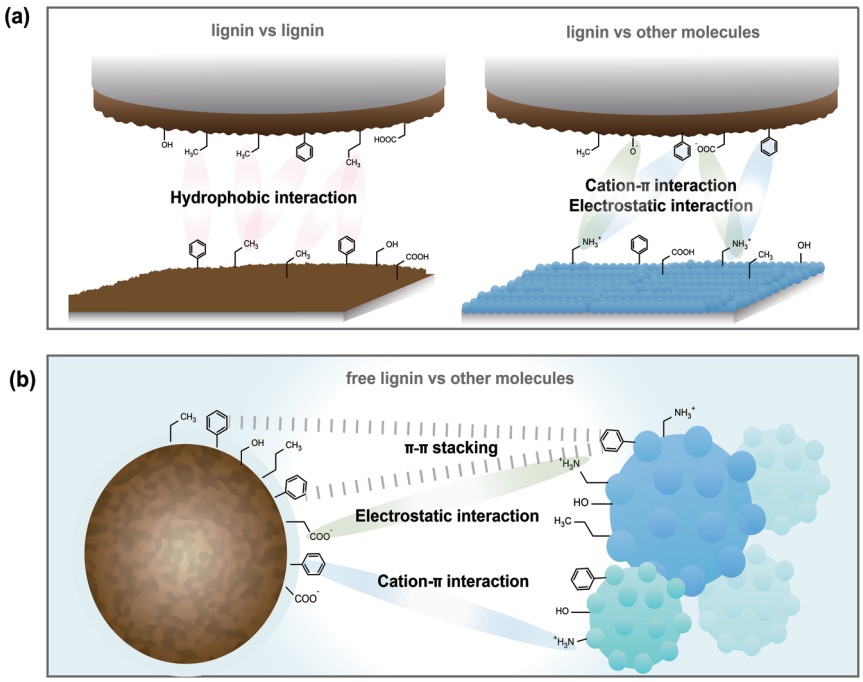

Fig. 5 Graphical illustrations of the most dominant interactions of lignin. (a) Interaction mechanisms between two lignin surfaces (symmetric) and between a lignin surface and the surface of another molecule (asymmetric). (b) Interaction mechanism between free lignin and other molecules in a free solution.

SFA results, the cohesion between lignin films was a result of hydrophobic interactions, especially under the low pH conditions wherein lignin possesses sufficient hydrophobicity. In contrast, when the lignin nanofilm interacted with other surfaces/molecules (*i.e.*, any surface or molecules capable of binding to lignin other than lignin itself, including –OH, –COOH, $–CH_3$, $–NH_2$ groups or aromatic rings), the electrostatic attraction (between the negatively charged lignin surface

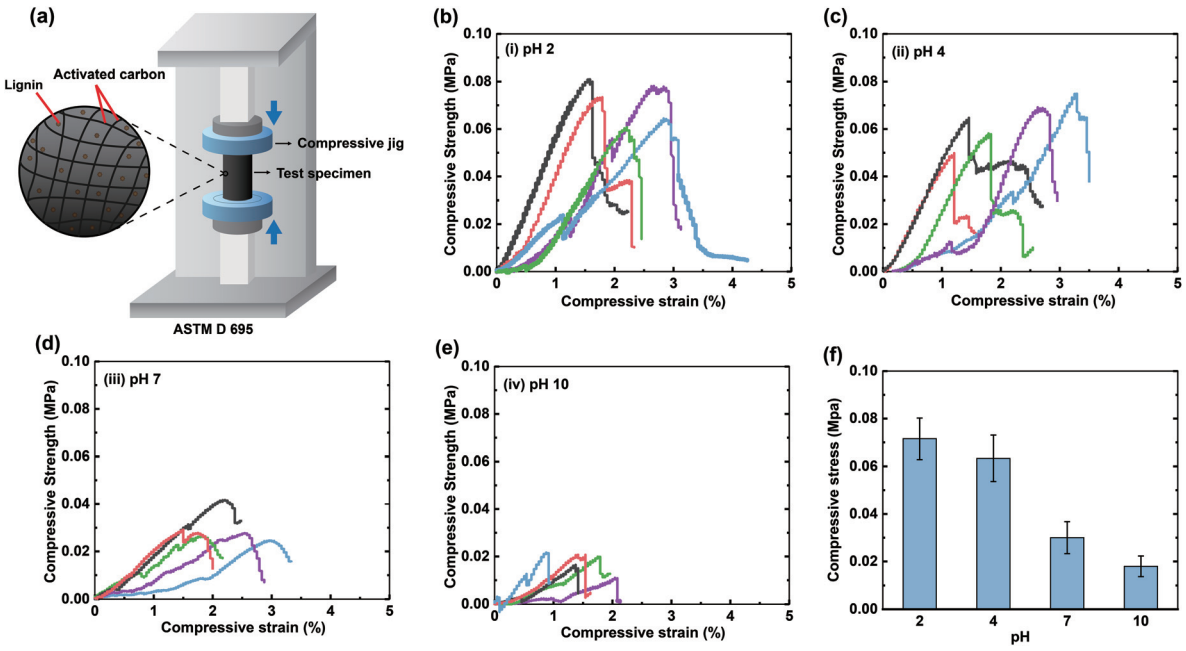

Fig. 6 Setup for testing the compressive strength of activated carbon–lignin composites using a universal testing machine. Compressive stress–strain curves of activated carbon–lignin composites in pH conditions of (b) pH 2, (c) pH 4, (d) pH 7, and (e) pH 10; different colors indicate repeated measurements. (f) Summary of the average compressive stress values.

and some positively charged surface) and cation–π interactions (in which lignin functions as a π source and the other surface functions as a cation source) are more dominant than other interactions (such as hydrophobic interactions and hydrogen bonding) (Fig. 5a). In the case of free lignin interactions (when lignin was dissolved in a good solvent), π–π interactions are the dominant type of interaction from lignin, as demonstrated by QCM-D measurements (Fig. 5b). This observation implies that lignin exhibits different adhesion mechanisms depending on its state (*i.e.*, fixed on a surface or free in a solution). In other words, the orientational freedom and/or mobility of lignin are one of the key factors determining its adhesion efficacy.

Activated carbon–lignin composite fabrication

We next demonstrated that the measured nanoscopic interactions can be extended to the bulk macroscopic properties of lignin-based materials by fabricating activated carbon–lignin composites. A previous study have demonstrated the compositing activated carbon with lignin enhanced the compressive strength of the carbon.[20] In contrast, the increase in the ion concentration hindered interfacial interactions between the lignin molecules and carbon composites, thereby reducing the compressive strength. In this study, activated carbon–lignin composites were prepared under different pH conditions. Fig. 6b–e show the corresponding stress–strain curves; the highest compressive strength (~56.17 kPa) occurred at pH 2, and the compressive strength decreased with the increasing pH of the buffer solution to ~19.58 kPa at pH 10 (Fig. 6f). This trend was identical to that observed in the SFA results, in which the adhesion between lignin and CH_3-SAM decreased owing to hydrophobic interactions. Specifically, as the pH increased, the hydrophobic interactions between the lignin and activated carbon molecules decreased, followed by internal fracturing of the composites at low compressive stress conditions. Therefore, the pH conditions of the slurry must be considered when enhancing the strength of activated carbon–lignin composites.

Conclusions

The interaction forces between lignin and functionalized SAMs (OH, COOH, C_6H_5, CH_3, NH_2) in different pH conditions were evaluated through SFA and QCM-D measurements. The following conclusions were derived:

(i) The adhesive strength of lignin nanofilms generally decreased with increasing pH except in cases involving surfaces/molecules with primary amine groups.

(ii) The lignin nanofilms could effectively interact *via* electrostatic and cation–π interactions with positively charged surfaces/molecules.

(iii) The cohesion mechanism of lignin nanofilms was primarily attributed to hydrophobic interactions.

(iv) Free lignin (dissolved in a good solvent) dominantly interacted with surfaces/molecules with π groups *via* π–π stacking.

(v) The nanoscale adhesion force measurements could be successfully extrapolated to the macroscale, as indicated by the compressive strength evaluation of activated carbon/lignin composites.

Notably, this study examined a specific type of lignin, *i.e.*, sulfonated alkaline lignin. Different conclusions may be derived with lignin from different botanic origins and/or isolation processes. Nevertheless, this fundamental study of lignin interaction mechanisms is expected to provide insights into the binding and assembly mechanism of lignin, which is expected to promote its use as an eco-friendly and organic-solvent-free material in the near future.

Conflicts of interest

There are no conflicts to declare.

Acknowledgements

This work was supported by the Basic Science Research Program (2019R1A2C2005854), the Technology Development Program to Solve Climate Changes (2017M1A2A2087630) through the National Research Foundation of Korea (NRF) funded by the Ministry of Science of Korea. This work was also supported by the Ministry of Trade, Industry & Energy/Korea Institute of Energy Technology Evaluation and Planning (MOTIE/KETEP) (20214000000660) and the 2021 Research Fund (1.200033.01) of Ulsan National Institute of Science and Technology (UNIST). Additionally, this work was supported by the Technology Innovation Program (20013963, XDI related special chemical product manufacturing and high value added material parts application technology development) funded by the Ministry of Trade, Industry & Energy (MOTIE, Korea). We thank Prof. Sebyung Kang at UNIST for providing QCM-D equipment.

Notes and references

1 W. Boerjan, J. Ralph and M. Baucher, *Annu. Rev. Plant Biol.*, 2003, **54**, 519–546.
2 T. Q. Hu, *Chemical modification, properties, and usage of lignin*, Springer, 2002.
3 H. Hatakeyama and T. Hatakeyama, *Biopolymers*, 2009, 1–63.
4 J. Ralph, C. Lapierre and W. Boerjan, *Curr. Opin. Biotechnol.*, 2019, **56**, 240–249.
5 P. Figueiredo, K. Lintinen, J. T. Hirvonen, M. A. Kostiainen and H. A. Santos, *Prog. Mater. Sci.*, 2018, **93**, 233–269.
6 W. Thielemans, E. Can, S. Morye and R. Wool, *J. Appl. Polym. Sci.*, 2002, **83**, 323–331.
7 P. Figueiredo, K. Lintinen, A. Kiriazis, V. Hynninen, Z. Liu, T. Bauleth-Ramos, A. Rahikkala, A. Correia, T. Kohout and B. Sarmento, *Biomaterials*, 2017, **121**, 97–108.

8 S. H. Ghaffar and M. Fan, *Int. J. Adhes. Adhes.*, 2014, **48**, 92–101.
9 X. Ouyang, L. Ke, X. Qiu, Y. Guo and Y. Pang, *J. Dispersion Sci. Technol.*, 2009, **30**, 1–6.
10 A. J. Ragauskas, G. T. Beckham, M. J. Biddy, R. Chandra, F. Chen, M. F. Davis, B. H. Davison, R. A. Dixon, P. Gilna, M. Keller, P. Langan, A. K. Naskar, J. N. Saddler, T. J. Tschaplinski, G. A. Tuskan and C. E. Wyman, *Science*, 2014, **344**, 1246843.
11 V. K. Thakur, M. K. Thakur, P. Raghavan and M. R. Kessler, *ACS Sustainable Chem. Eng.*, 2014, **2**, 1072–1092.
12 L. Dai, R. Liu, L.-Q. Hu, Z.-F. Zou and C.-L. Si, *ACS Sustainable Chem. Eng.*, 2017, **5**, 8241–8249.
13 B. Jiang, C. Chen, Z. Liang, S. He, Y. Kuang, J. Song, R. Mi, G. Chen, M. Jiao and L. Hu, *Adv. Funct. Mater.*, 2020, **30**, 1906307.
14 C.-J. Liu, *Mol. Plant*, 2012, **5**, 304–317.
15 V. K. Thakur and M. K. Thakur, *Int. J. Biol. Macromol.*, 2015, **72**, 834–847.
16 M. P. Pandey and C. S. Kim, *Chem. Eng. Technol.*, 2011, **34**, 29–41.
17 S. Laurichesse and L. Avérous, *Prog. Polym. Sci.*, 2014, **39**, 1266–1290.
18 W. Zhao, B. Simmons, S. Singh, A. Ragauskas and G. Cheng, *Green Chem.*, 2016, **18**, 5693–5700.
19 J. Israelachvili, Y. Min, M. Akbulut, A. Alig, G. Carver, W. Greene, K. Kristiansen, E. Meyer, N. Pesika and K. Rosenberg, *Rep. Prog. Phys.*, 2010, **73**, 036601.
20 Y. Song, J. Park, C. Lim and D. W. Lee, *ACS Sustainable Chem. Eng.*, 2019, **8**, 362–371.
21 P. Azadi, O. R. Inderwildi, R. Farnood and D. A. King, *Renewable Sustainable Energy Rev.*, 2013, **21**, 506–523.
22 L. Chai and J. Klein, *Langmuir*, 2007, **23**, 7777–7783.
23 M. Valtiner, S. H. Donaldson Jr., M. A. Gebbie and J. N. Israelachvili, *J. Am. Chem. Soc.*, 2012, **134**, 1746–1753.
24 K. L. Johnson, K. Kendall and A. Roberts, *Proc. R. Soc. London, Ser. A*, 1971, **324**, 301–313.
25 G. Sauerbrey, *Z. Phys.*, 1959, **155**, 206–222.
26 E. Melro, A. Filipe, A. J. M. Valente, F. E. Antunes, A. Romano, M. Norgren and B. Medronho, *Int. J. Biol. Macromol.*, 2020, **164**, 3454–3461.
27 G. A. A. Saracino, R. Improta and V. Barone, *Chem. Phys. Lett.*, 2003, **373**, 411–415.
28 Z. Adamczyk, M. Zaucha and M. Zembala, *Langmuir*, 2010, **26**, 9368–9377.
29 A. E. Kazzaz and P. Fatehi, *RSC Adv.*, 2020, **10**, 36778–36793.
30 N. J. Singh, S. K. Min, D. Y. Kim and K. S. Kim, *J. Chem. Theory Comput.*, 2009, **5**, 515–529.
31 Z. Aliakbar Tehrani and K. S. Kim, *Int. J. Quantum Chem.*, 2016, **116**, 622–633.
32 S. Guriyanova and E. Bonaccurso, *Phys. Chem. Chem. Phys.*, 2008, **10**, 4871–4878.
33 J. N. Israelachvili, *Intermolecular and surface forces*, Academic press, 2015.